THE ASTROPHYSICAL JOURNAL, 466:392–403, 1996 July 20

WIND INHOMOGENEITIES IN WOLF-RAYET STARS. I. SEARCH FOR SCALING LAWS USING WAVELET TRANSFORMS

SÉBASTIEN LÉPINE AND ANTHONY F. J. MOFFAT
Département de Physique, Université de Montréal C.P. 6128, Succ. Centre-Ville, Montréal, QC, Canada H3C 3J7,
and Observatoire du Mont-Mégantic; lepine@astro.umontreal.ca, moffat@astro.umontreal.ca

AND

R. N. HENRIKSEN[1]
Astronomy group; Department of Physics, Queen's University, Kingston, ON, Canada K7l 3N6; henriksn@astro.queensu.ca
Received 1995 November 27; accepted 1996 February 8

ABSTRACT

We describe a new technique involving wavelet transforms for analyzing discrete stochastic components like those found on the tops of emission lines in Wolf-Rayet stars. A *wavelet power spectrum* is used to characterize the variable component of the emission line we believe arises from the superposition of many individual Gaussian-like subpeaks. This was applied to emission-line spectra of eight Wolf-Rayet stars obtained at the Canada-France-Hawaii Telescope and European Southern Observatory. Where the data show the most power we identify a *dominant scale*, which is found to be very similar in all but one of the stars in our sample.

We present a phenomenological model where the variable structure on top of the emission line is represented by a sum of individual subpeaks of the same simple shape (Gaussian or triangular) and various scales. This model is used to introduce the idea of *scaling laws*. The amplitude A and number density N of subpeaks on a given scale are related to their characteristic width σ (i.e., velocity dispersion) by scaling relations, of which the simplest form is a power law: $A \sim \sigma^{\alpha}$ and $N \sim \sigma^{\beta}$. The wavelet power spectrum is used to verify the consistency of this model with the data. Synthetic signals are generated, and their wavelet spectra are compared to those of the data. This provides a constraint on the value of $2\alpha + \beta$, which is found to be $\approx 2.7 \pm 0.5$(s.d.) for the model involving Gaussians, or $\approx 3.4 \pm 0.6$(s.d.) for the model involving triangles. The implications provided by this new constraint are discussed.

Subject headings: radiative transfer — stars: mass loss — stars: Wolf-Rayet — waves

1. INTRODUCTION: WHY USE WAVELETS?

It was already suggested by Antokhin, Kholtygin, & Cherepashchuk (1988), on the basis of *indirect* evidence by Cherepashchuk, Eaton, & Khaliullin (1984), that the strong stellar winds of Wolf-Rayet stars could be made up of dense clouds immersed in a rarefied intercloud medium. Attempts were made by Antokhin, Nugis, & Cherepashchuk (1992) to reproduce He line profiles using an inhomogeneous wind model. Likewise, the need for some kind of *clumping* in the wind of Wolf-Rayet stars in order to reproduce electron scattering wings better was pointed out by Hillier (1991). He showed that an inhomogeneous wind required lower mass-loss rates than a homogeneous wind to reproduce line strengths accurately.

Systematic *direct* observation of variable subpeaks on the tops of broad emission lines in Wolf-Rayet stars was first made by Moffat et al. (1988) and McCandliss (1988). An extensive study of emission-line subpeaks in many Wolf-Rayet stars of different subclass was then carried out by Robert (1992). Careful analysis of individual subpeaks identified in the latter work, combined with simple physical assumptions, led Moffat et al. (1994) to suggest a phenomenological model for the inhomogeneous component of the wind using scaling laws. This was used by Moffat & Robert (1994) to suggest a possible factor ~ 3 decrease in mass-loss estimates in Wolf-Rayet winds based on common density-squared dependent emission mechanisms, on the assumption of a fully clumped wind. A review of the observation of inhomogeneities and the information they can provide about the wind was made by Brown et al. (1995).

This paper is an attempt to test the assumption of scaling laws in the inhomogeneous component of Wolf-Rayet winds, as revealed by the presence of subpeaks on the tops of emission lines. Wavelet analysis techniques are developed and used to compare the observations to a simple phenomenological model involving scaling laws.

In previous work that led to the scaling-law hypothesis (Robert 1992; Moffat et al. 1994), individual structures were identified and extracted using multi-Gaussian fits and wavelet convolutions, respectively. A statistical analysis of these extracted structures then uncovered relations reminiscent of those used in describing supersonic compressible turbulence in giant molecular clouds (e.g., Henriksen 1991), where full-scale clumping is thought to be the rule. However, because they arise in an optically thin medium (the outer part of the wind) and because they are assumed to be distributed with spherical symmetry around the star, the spectroscopic subpeaks in Wolf-Rayet emission lines are always seen in *projected velocity* space and are subjected to superposition effects. For example, two spatially distinct inhomogeneities could have the same *projected* velocity and thus appear as a single subpeak in the spectrum. This effect can introduce a bias in the statistical analysis involving extracted *apparent* subpeaks, because several spatially distinct inhomogeneities with a small velocity dispersion (σ_v) may appear as a single (unresolved) subpeak having larger σ_v in projected velocity space. Possibly, one might benefit from using a technique that avoids the identification of indi-

[1] On leave at Service d'Astrophysique, C.E.N. Saclay, F-91191 Gif-sur-Yvette Cedex, France.

vidual structures, being sensitive only to the general profile produced by a collection of subpeaks.

Another problem is the presence of instrumental and statistical *noise*. When extracting individual structures, the noise may artificially introduce a large number of small-scale features. These would be difficult to distinguish from real small-scale subpeaks. Not knowing exactly the threshold for intrinsic small-scale structure identification is a problem, because scaling relations depend critically on the presence of small-scale components.

In an attempt to avoid these pitfalls (i.e., noise and superposition effects), a wavelet analysis method is developed to study the variable components of WR emission lines.

The *wavelet transform* is a technique, analogous to the Fourier transform for periodic data, that is well-adapted to the study of nonperiodic variable signals. In astronomy, it has found applications in the study of time series photometry of variable stars (Szatmáry, Vinkó, & Gál 1994), and in the study of hierarchical structures in molecular clouds (Gill & Henriksen 1990), and galaxy distributions (Slezak, De Lapparent, & Bijaoui 1993; Martínez, Paredes, & Saar 1993). It is also used as an objective, multiscale structure identifier (Slezak, Durret, & Gerbal 1994).

In the present study, the wavelet transform is used to evaluate the *wavelet power spectrum*, which can give valuable statistical information on a random distribution of subpeaks, including any additional feature such as noise. The method leads to a clear identification of the noise threshold. The power spectrum is then used as a comparative tool for testing phenomenological models involving scaling laws. This adds new constraints on the clumping hypothesis for Wolf-Rayet winds. We discuss how new observations should be carried out in order to confront existing models better.

2. THE WAVELET ANALYSIS

About 12 years ago, wavelet transforms began to be used as an alternative to Fourier transforms in the case of nonperiodic signals (see Farge 1992; Daubechies 1992). The advantage of wavelets as analyzing functions is that they are well localized in space, as opposed to Fourier-based functions (sine waves) that oscillate indefinitely over all space. Two conditions must be fulfilled by some real function $\psi(x)$, in order for it to be used as a wavelet: (1) its mean must be zero, i.e.,

$$\int_{-\infty}^{\infty} \psi(x)dx = 0 ,$$

and (2) it must be well localized in space.

A commonly used wavelet (e.g., Argoul et al. 1989) is the so-called *Mexican hat*, which is the second derivative of a Gaussian:

$$\psi(x) = (1 - x^2)e^{-x^2/2} .$$

This function satisfies both the above conditions.

From the function $\psi(x)$, also known as the *mother wavelet*, we generate a *wavelet family* $\psi_{b,a}(x)$ by successive *translation* (parameter b) and *dilation* (parameter a) of the mother wavelet, i.e.,

$$\psi_{b,a}(x) = \frac{1}{a}\psi\left(\frac{x-b}{a}\right) .$$

This is analogous to the definition of the Fourier function, which is expressed in terms of variations in *phase* and *frequency* in a convolution with a sine wave. However, precise information about the exact *location* of a feature can be obtained concisely when using a wavelet basis. A Fourier basis needs an infinitely broad spectral regime.

The *continuous wavelet transform* $\tilde{f}(b, a)$ of a one-dimensional signal $f(x)$ using a wavelet family $\psi_{b,a}(x)$ is simply

$$\tilde{f}(b, a) = \int_{-\infty}^{\infty} f(x)\psi_{b,a}(x)dx . \quad (1)$$

Its inverse is given by the *wavelet reconstruction theorem*:

$$f(x) = \frac{1}{C_\psi}\int_{-\infty}^{\infty}\int_{0}^{\infty} \tilde{f}(b, a)\psi\left(\frac{x-b}{a}\right)\frac{da\,db}{a} . \quad (2)$$

The quantity C_ψ is a constant determined by the choice of mother wavelet form:

$$C_\psi = 2\pi\int_{0}^{\infty} \xi^{-1}|\hat{\psi}(\xi)|^2 d\xi .$$

Here we denote $\hat{\psi}(\xi)$ as the Fourier transform of $\psi(x)$:

$$\hat{\psi}(\xi) = \frac{1}{\sqrt{2\pi}}\int_{-\infty}^{\infty} e^{-ix\xi}\psi(x)dx .$$

Note that the continuous wavelet transform of a one-dimensional signal is expressed in two dimensions. As a consequence, there is some redundancy of information in *wavelet space*, i.e., a single subpeak of a given scale shows a wavelet response over neighboring scales (see Fig. 1). This redundancy turns out to be useful, however, because for some specific wavelet families the signal can be reconstructed from its wavelet transform using a different mother wavelet function (see Daubechies 1992). For the Mexican-hat family, the delta function can be used as a reconstruction basis, thus making the reconstruction theorem simpler:

$$f(x) = \frac{1}{C'_\psi}\int_{-\infty}^{\infty}\int_{0}^{\infty} \tilde{f}(b, a)\delta(x - b)\frac{da\,db}{a}$$

$$= \frac{1}{C'_\psi}\int_{0}^{\infty} \tilde{f}(x, a)\frac{da}{a} , \quad (3)$$

with the normalization constant becoming

$$C'_\psi = 2\pi\int_{0}^{\infty} \xi^{-1}\hat{\psi}(\xi)\hat{\delta}(\xi)d\xi = \sqrt{2\pi}\int_{0}^{\infty} \xi^{-1}\hat{\psi}(\xi)d\xi .$$

The wavelet transform is in many ways comparable to the *windowed Fourier transform* (WFT), but much more efficient. We recall that the WFT is obtained by using the Fourier transform over some restricted domain of a signal, as defined by some aperture, the so-called *window*. The position of this window can be used as an extra parameter, keeping information about location while a local determination of Fourier coefficients is made. The main problem with the WFT is that the arbitrarily chosen size of the window is kept constant. Obviously, some advantage would be gained if we could automatically adapt the size of the window with the frequency of the analyzing function, for

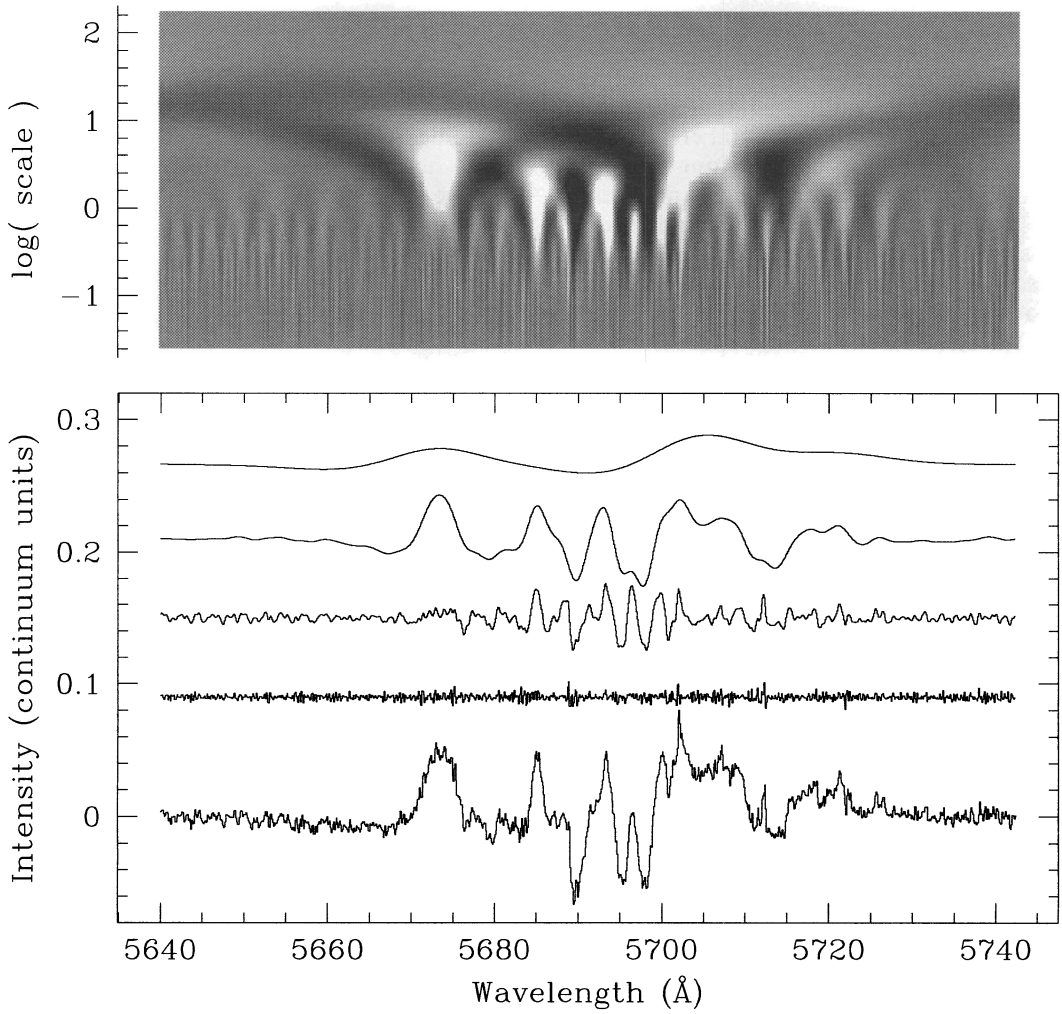

FIG. 1.—*Top*: Wavelet transform of a difference spectrum of the star WR 137. *Bottom*: Same difference spectrum (*bottom curve*) decomposed into different scale components by using wavelet filtering. Upward from the bottom curve are integrations of the wavelet transform over scale intervals (in Å) [a1, a2] = [0.02, 0.13], [0.13, 0.8], [0.8, 5.0], and [5.0, 32.0], respectively.

example by optimizing the wavenumber (k)–position (x) uncertainty relation $\Delta x\,\Delta k = 2\pi$. This is what the wavelet transform achieves; it is an improved WFT in which the size of the window (the scale) is *automatically* adapted to the frequency used.

Wavelet transforms can also be described as passband frequency filters. Filtering properties can be inferred from the wavelet reconstruction theorem: instead of integrating over the domain $0 < a < \infty$ (eq. [3]), one could integrate over any interval $a1 < a < a2$. This removes the components of the signal having scales outside this interval (see Fig. 1). This capacity of zooming in to any given scale, only keeping components relevant to that scale, leads to applications in fractal analysis.

If exact information about location is of no great relevance (e.g., features are randomly distributed), scaling information may be easily obtained using the *wavelet power spectrum* (WPS). We define the wavelet power spectrum $W_{b1,b2}(a)$ of any function $f(x)$ over some spatial domain [$b1$, $b2$] as the integration of the square of the wavelet transform over that domain:

$$W_{b1,b2}(a) = \int_{b1}^{b2} [\tilde{f}(b, a)]^2\, db\ . \qquad (4)$$

The dependence of $W_{b1,b2}$ on the parameter a will be used to characterize the scaling behavior of the function $f(x)$ over the spatial domain [$b1$, $b2$].

3. SCALED DISTRIBUTIONS AND THE POWER SPECTRUM

Wavelet analysis will be especially efficient when one has a signal made up of discrete components of various sizes. This appears to be the case for the variable component on top of Wolf-Rayet emission lines (Robert 1992). From the data, however, it is unclear if and how these components are organized. We attempt to model the data using the simplest phenomenological approach that comes to mind. Our model describes the signal as arising from a sum of randomly distributed Gaussian-like subpeaks having different widths and amplitudes.

Let $I(x)$ be a signal arising from the superposition of N Gaussian-like structures having some fundamental shape $g(x)$. Let these structures be parameterized by their individual width σ_j, intensity amplitude A_j, and location x_{ij}. If we assume that we have N_j structures of width σ_j, then

$$I(x) = \sum_j \sum_{i=1}^{N_j} A_j\, g\left(\frac{x - x_{ij}}{\sigma_j}\right). \qquad (5)$$

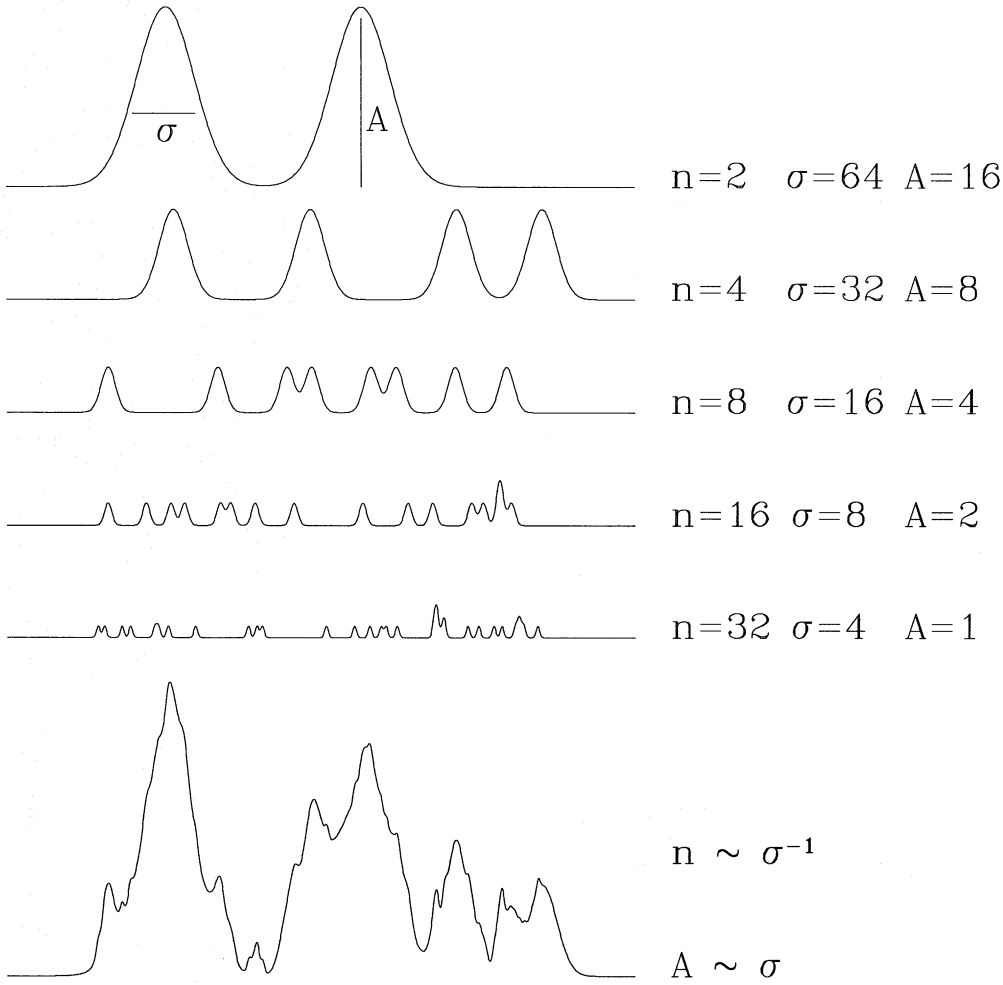

FIG. 2.—Example construction of a synthesized subpeak profile (*bottom*) using simple scaling relations. At different scales, Gaussians are randomly placed, with their number n and intensity amplitude A determined by the scaling relations. The resulting profile is the sum of the individual scales. This example corresponds to parameters $\alpha = 1$ and $\beta = -1$ (see text).

Here we have made the simplifying assumption that all N_j structures with width σ_j have the same amplitude A_j (e.g., Fig. 2).

It appears plausible to describe this signal using simple, general *scaling relations*. Assuming a continuous distribution over all possible scales σ, we may rewrite $[A_j, N_j]$ as $[A(\sigma), N(\sigma)]$ and use scaling relations such as the power laws

$$A(\sigma) = K_A \sigma^{\alpha} , \quad (6)$$

$$N(\sigma) = K_N \sigma^{\beta} , \quad (7)$$

which are dependent on the four parameters K_A, α, K_N, and β.

Given the conclusions from the previous studies of Wolf-Rayet emission-line subpeaks (Robert 1992; Moffat et al. 1994; Moffat & Robert 1994) this is reasonable as a working model, to the extent that no difficulties have been encountered yet with it. Previous estimates led to $\alpha \approx 1.0$, $\beta \approx -3.6$, for the extracted subpeaks.[2] We will now show how α and β can be more objectively constrained using the WPS.

The total flux $F(\sigma)d\sigma$ emitted by all the blobs in the range $[\sigma, \sigma + d\sigma]$ should, according to our model, correspond to

$$F(\sigma)d\sigma = N(\sigma)A(\sigma)\sigma\, d\sigma = K_A K_N \sigma^{\alpha+\beta+1}\, d\sigma . \quad (8)$$

However, we do not expect the piling up of a large number of structures in a signal to be directly detected by the wavelet analysis—only the resulting deviations from the mean. This can be understood by noticing that the wavelet transform of a single Gaussian has zero mean. Because it is a linear transformation, the wavelet transform of a set of superposed Gaussians is the sum of their individual wavelet transforms. So the overall wavelet transform should also have zero mean, with a mean deviation proportional to the square root of the number of Gaussians involved. This mean deviation is what the wavelet transform will be sensitive to.

Thus, the WPS (eq. [4]) gives us information about the squared amplitude of the *mean deviation* at some scale σ. In the range of scales $[\sigma, \sigma + d\sigma]$, this should be directly proportional to the square of (1) the intensity amplitude $A(\sigma)$ of individual structures at that scale and (2) the square root of $N(\sigma)$, the number density of structures at the same scale. Naively, we might expect the WPS to show a dependence

[2] From the scaling relations $f \sim \sigma^{2.0 \pm 0.4(\text{s.d.})}$ (Moffat et al. 1994) and $N(f) \sim f^{-2.3 \pm 0.8(\text{s.d.})}$ (Robert 1992), where $f = A\sigma$. The standard deviation (s.d.) is based on the scatter for a typical star for $f(\sigma)$ and among several stars for $N(f)$. One finds $A \sim \sigma^{1.0 \pm 0.4(\text{s.d.})}$ and $N(\sigma) \sim \sigma^{-3.6 \pm 0.8(\text{s.d.})}$, i.e., $\alpha = 1.0 \pm 0.4$(s.d.); $\beta = -3.6 \pm 1.6$(s.d.).

such as

$$W(\sigma)d\sigma \sim [A(\sigma)\sqrt{N(\sigma)}]^2\, d\sigma = K_A^2 K_N \sigma^{2\alpha+\beta}\, d\sigma\ .$$

In fact, the WPS also includes information about the fundamental shape $g(x)$ of individual elements, since each element is itself a superposition of different scales. Strictly speaking, the WPS is a convolution of the general scaling laws with the WPS of an individual structure. Thus, the dependence on the parameters α and β will be more generally given by

$$W(\sigma) \sim \sigma^{\phi(2\alpha+\beta)}\ , \qquad (9)$$

where $\phi(2\alpha + \beta)$ is some nontrivial, but monotonic function that depends on the fundamental shape of the structures involved.

In order to check these ideas, we generated numerous signals with known scaling parameter values, according to the model described in equations (5), (6), and (7). For each synthetic signal, the WPS was evaluated and the power index $\phi = \phi(2\alpha + \beta)$ was determined (see Figs. 3 and 4). Simulations were done using both Gaussians and triangles as the fundamental shape. The function ϕ is shown to be significantly dependent on the choice of the fundamental shape $g(x)$, and this should be kept in mind.

In principle, we now have a way of obtaining the value of $2\alpha + \beta$ from the power spectrum by evaluating ϕ. There is some uncertainty in the evaluation of ϕ that arises from the fact that we are dealing with signals extended over a limited spatial domain, because subpeaks are then finite in number, and subjected to statistical variations. This explains the dispersion of the points in Figure 4 (simulated signals from which this figure was made, had a limited spatial extension of 500 units, to match that of the data). Another uncertainty arises from our poor knowledge of the fundamental shape of the structures in the data. This effect is rather limited for small values of $2\alpha + \beta$, but is far from negligible for large values, as seen in Figure 4. Other fundamental shapes (e.g., Lorenzians; rectangular profiles) were tested and found to give results similar to, or intermediate between, triangles and Gaussians.

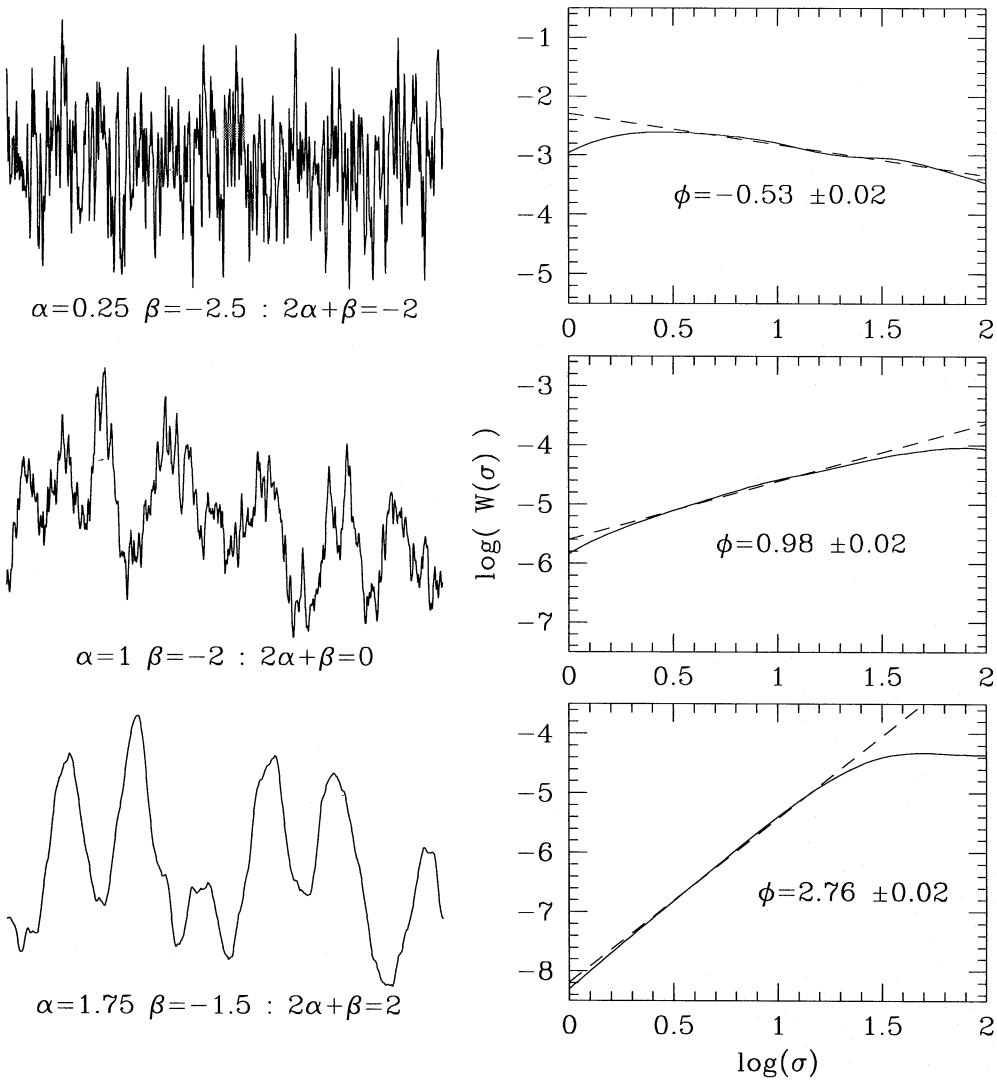

FIG. 3.—Wavelet power spectrum $W(\sigma)$ (*right column, solid line*) is plotted for each set of simulated multi-Gaussian signals depicted as examples on the left. These simulated subpeak distributions are scaled with different values of the parameters α and β. Notice that $W(\sigma)$ is very sensitive to these parameters: the power dependence of the WPS changes accordingly, giving different slopes ϕ (linear regression, *dotted line*), which can be used to obtain an estimate of $2\alpha + \beta$ (see Fig. 4). With this technique it is not possible to decouple α and β.

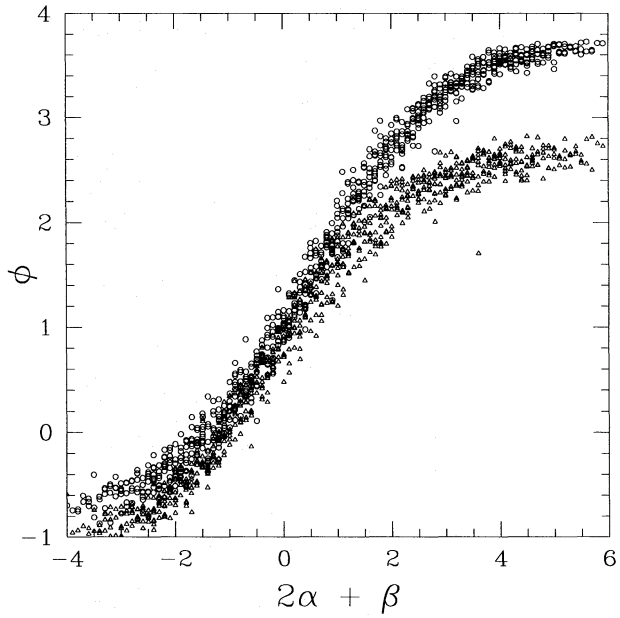

FIG. 4.—Power dependence of the WPS (slope ϕ in Fig. 3) given for different values of $2\alpha + \beta$, as obtained from simulations using the model described in the text. Results are shown for the use of Gaussians (*open circles*) and triangles (*open triangles*) as the fundamental shape of individual structures. Signals were generated using model parameters within the range $-1 < \alpha < 3$ and $-2 < \beta < -0.1$, each with a 0.1 step (2×820 models are thus shown here).

Notice also that very large absolute values of $2\alpha + \beta$ lead to asymptotic behavior in $\phi(2\alpha + \beta)$. An infinite value of $2\alpha + \beta$ would actually correspond to a case where no scaling laws are present (absence of small-scale elements). However, we see that it is not possible, with this method, to distinguish between that specific case and a case where $2\alpha + \beta \gtrsim 5$ (Gaussians) or $\gtrsim 4$ (triangles). Thus, we can say that evidence for scaling laws is only compelling when $|2\alpha + \beta|$ is found to be $\lesssim 4$.

4. DATA SOURCE

In order to test for consistency with the hypothesis of scaling laws in the subpeaks of observed emission-line profiles, it is necessary to have time-resolved, high spectral resolution, high signal-to-noise (S/N) data, to detect coherent structures over at least 1 order of magnitude in scale. We focus our attention on the best bank of high-resolution spectra to date: those obtained by A. F. J. M. and C. Robert in 1987, 1988, and 1989 (Robert 1992). These data consist of time-resolved, high-resolution, high S/N emission-line spectra from (1) the Canada-France-Hawaii Telescope (CFHT) (normal diffraction grating + Reticon at the coudé focus), showing mainly He II λ5412 in the WN stars HD 191765 (WN6), HD 192163 (WN6), and HD 193077 (WN5 + OB), and C III λ5696 for the WC stars HD 192103 (WC8), HD 192641 (WC7 + abs), and HD 193793 (WC7 + O4–5V); and (2) European Southern Observatory (ESO) (echelle + CCD at the Cassegrain focus), also showing C III λ5696 (among other lines) for the stars HD 164270 (WC9) and HD 165763 (WC5). These Wolf-Rayet stars are also designated as WR 134, WR 136, WR 138, WR 135, WR 137, WR 140, WR 103, and WR 111, respectively (van der Hucht et al. 1981); the latter names will be used hereafter in this paper. ESO spectra of the stars HD 96548 (WN8) and HD 113904 (WC6 + O9.5 Iab) from the same observing run were not included in this study: most emission lines of the former are perturbed by P Cygni edges, while emission lines of the latter are strongly diluted by the supergiant companion. These effects made the identification of variable subpeaks more problematic. CFHT observations of the two remaining bright WR stars in Cygnus, WR 133(WN5 + O9 Iab) and WR 139(WN5 + O6), were not included either: their emission lines are also heavily diluted or perturbed by their bright O companions. WR 137, 138, and 140 are also binaries, but of very long period (Annuk 1991) and dilution effects are less important, especially for WR 137 and WR 138.

All the spectra have a dispersion of ~0.1 Å per pixel and a signal-to-noise ratio per pixel in the continuum between 150 and 380 (see Table 1). Figure 5 shows a typical profile obtained for each star. The observations were made over an interval of 3–4 consecutive nights. Four to twelve spectra spaced by ~1 hr were obtained each night for each star. All spectra have been rectified.

The presence of subpeaks on the lines is obvious on the top of all flat-top emission lines (see Fig. 5). However, in the sloping part of a line profile it is often difficult to distinguish these narrow features. As a way to enhance the presence of discrete variable subpeaks, we have therefore subtracted the smoothed mean profile (based on the data from all three or four nights) from each line in each star, as was done by Robert (1992). In order to avoid degradation of the base profile in the smoothing process, we used optimized sixth-order Savitzki-Golay smoothing filters. The time dependence of the resulting difference profiles is shown as an example in Figure 6 for one night's data. The persistence and slow evolution of the most obvious discrete features

TABLE 1

LIST OF OBSERVED EMISSION LINES

Star	HD	Subtype	v_∞[a] (km s^{-1})	Number of Spectra	S/N_{cont}	Line	⟨EW⟩ (Å)[b]
WR 103.....	164270	WC9	1190	30	210	C III λ5696	−294.2
WR 111.....	165753	WC5	2415	28	150	C III λ5696	−67.9
WR 134.....	191765	WN6	1905	36	190	He II λ5411	−69.6
WR 135.....	192103	WC8	1405	26	180	C III λ5696	−247.6
WR 136.....	192163	WN6	1605	26	200	He II λ5411	−62.8
WR 137.....	192641	WC7 + OB	2550	25	240	C III λ5696	−83.8
WR 138.....	193077	WN5 + OB	1345	18	230	He II λ5411	−13.3
WR 140.....	193793	WC7 + O4–5	2900	23	380	C III λ5696	−77.6

[a] From Prinja et al. 1990.

[b] Time-averaged equivalent width from Robert 1992.

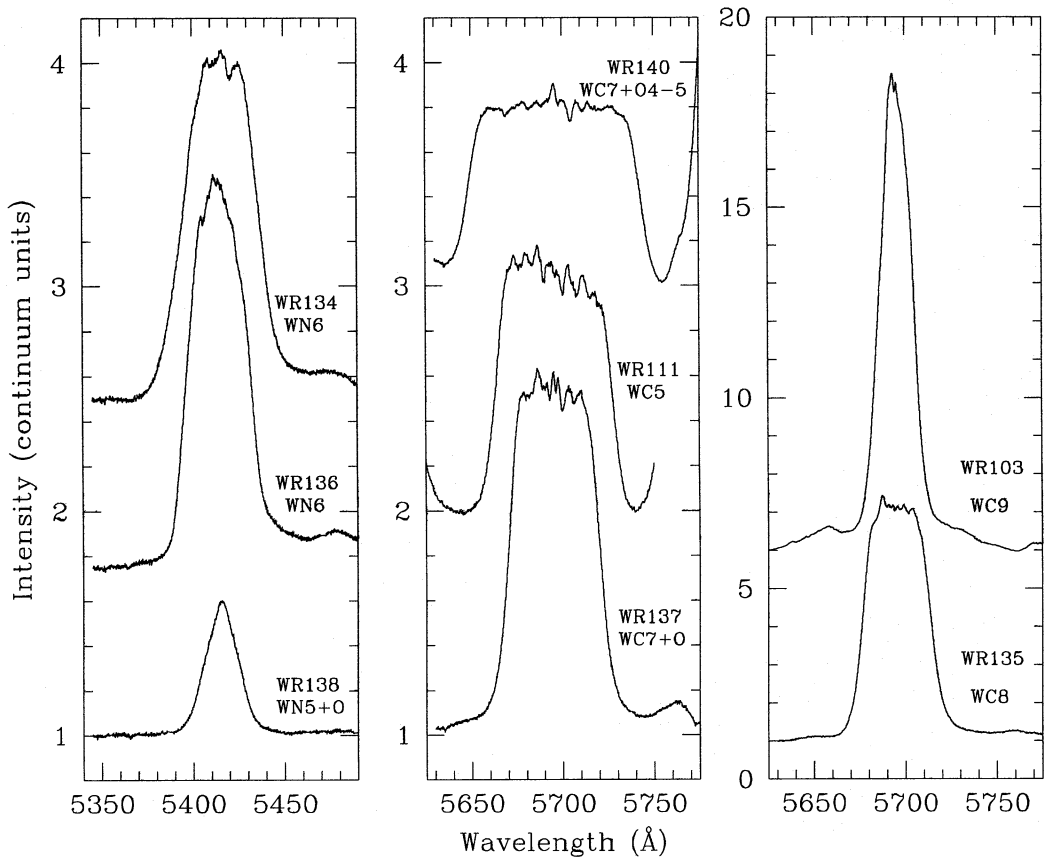

FIG. 5.—Individual sample spectra of emission lines in eight stars observed at ESO (WR 103, WR 111) and CFHT (rest). The He II λ5412 line was observed in the WN stars, C III λ5696 in the WC stars. All these lines show variable subpeaks, which are more obvious on flat-top lines.

makes it extremely unlikely for them to be the result of instrumental or statistical noise.

5. DATA ANALYSIS

5.1. *The Wavelet Power Spectrum Profile*

For each individual line (C III 5696 in WC stars, and He II 5411 in WN stars) in each spectrum of our eight Wolf-Rayet stars, we have evaluated the WPS of the structures observed on top of the bright emission lines. From the spectroscopic signal $I(\lambda)$ obtained after subtracting off the mean, we first calculate the wavelet transform $\tilde{I}(\lambda', \sigma)$. Then for an emission line at location λ_0 with a FWHM of $\Delta\lambda$, we evaluate $W(\sigma)$ over the restricted domain $[\lambda_0 - \Delta\lambda/2, \lambda_0 + \Delta\lambda/2]$, in order to avoid edge effects. For a given line in a given star we obtain the average WPS $\bar{W}(\sigma)$ from each of the different spectra. Then we normalize $\bar{W}(\sigma)$ by dividing by the mean line equivalent width for that star, in order to facilitate a comparison among different objects.

A sample average WPS so obtained for the C III 5696 line in the star WR 137 is shown in Figure 7. The smallest scales are usually dominated by instrumental or photon statistical noise, appearing as high-frequency components. The noise sets a minimal value for the power at a given scale. Intrinsic subpeaks in the signal may only be detected with confidence if they amount to a power greater than this minimal value set by the noise.

Beyond the region where noise dominates, we observe an increase in amplitude as the scale increases. A noise-only signal cannot produce such an increase in power for larger scales since it is always dominated by small-scale components. *This is the principal diagnostic for the presence of discrete structures distinct from the noise.* The rate of increase can be used to determine the presence of scaled distributions, as described in the previous section. However, one must be very careful to remove the possible effects that might arise from the presence of noise (see section below).

The WPS usually reaches a maximum at some scale we designate as the *dominant scale.* This usually corresponds to the scale at which the structures have the highest intensity amplitude in the signal. In our model of a scaled distribution, this dominant scale may be introduced by setting an upper limit for the width of any intrinsic individual structure. The shape of the WPS is very similar for all stars in our sample (Fig. 8). These are all consistent with the presence of intrinsic subpeaks, with various levels of superposed instrumental and statistical noise.

In this paper, we have neglected possible variations in the WPS across the emission line. This restriction was added only for the sake of our simple model, which does not include this behavior. However, such variations in the power spectrum were actually observed. These will be analyzed, along with the time dependence, in an upcoming paper (Lépine et al. 1996, hereafter Paper II).

5.2. *The Noise Limit*

Noise effects appear in the WPS as an excess on smaller scales. As a good approximation, the noise can be said to be independent of the behavior of the structures we are interested in since it arises mainly from photon statistics (dependent mainly on the amplitude in the emission line, which is large relative to the subpeaks) and from instrumen-

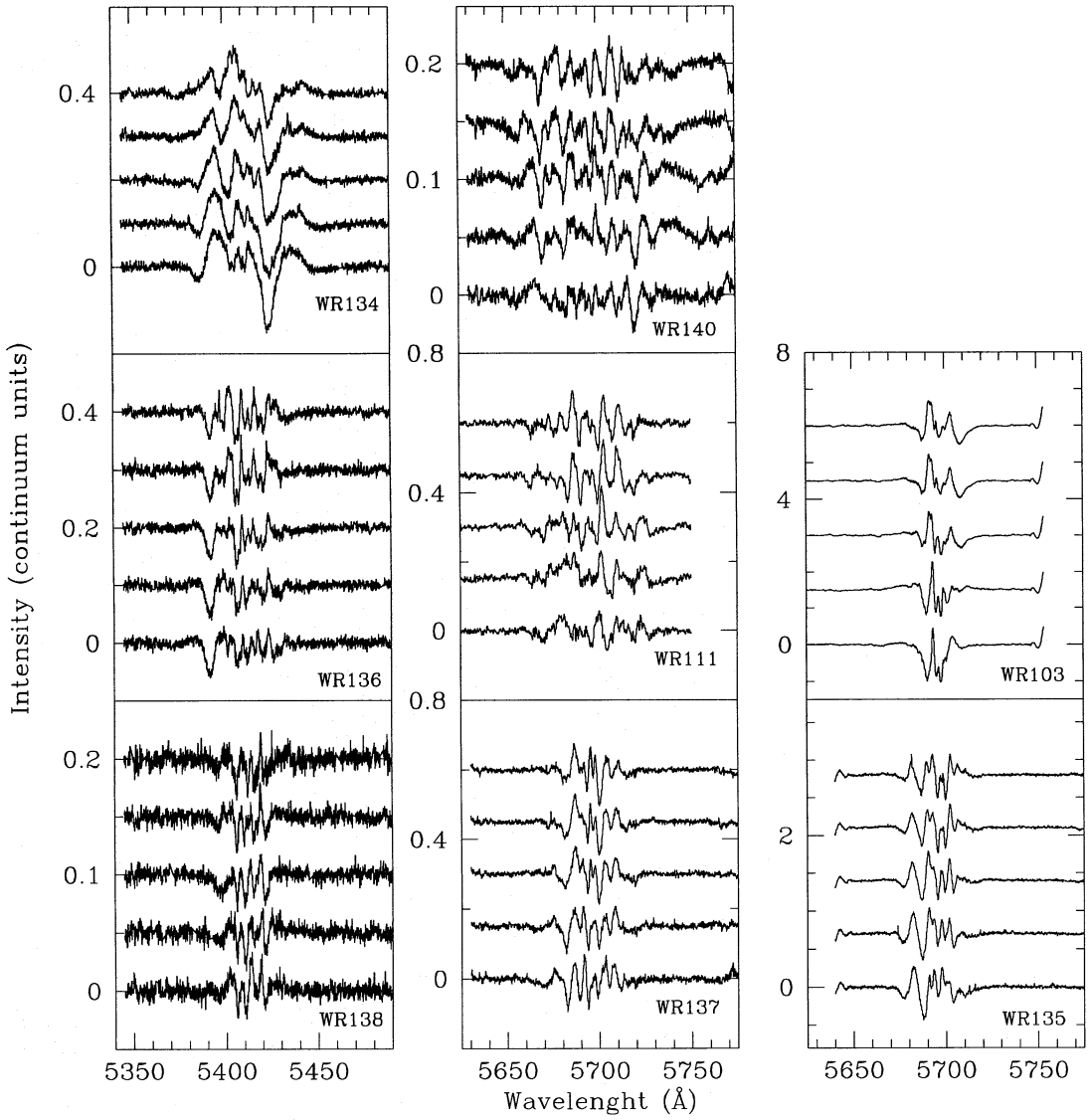

FIG. 6.—Set of five consecutive spectra taken from the same single night as the spectra in Fig. 5 is shown for each star. In each case, an average, smoothed line profile was subtracted in order to enhance the presence of the subpeaks. The average time separation is ~1 hr between successive spectra with time increasing upward. Some subpeaks appear to move slightly and change intensity with time.

tal, signal-independent readout noise. It is possible statistically to remove these noise effects by subtracting their power contribution from the WPS. This contribution can be evaluated by using the adjacent continuum emission of the star, which normally should be devoid of any significant intrinsic structure (i.e., it should be flat). However, both the photon count and the Poisson noise arising from it are lower in the continuum than in the line peak, so that the noise must be scaled accordingly. However, we need not evaluate any multiplicative factor, since it can be obtained directly from the WPS. If we assume that the noise has more or less the same scaling behavior in both the line and continuum, we need only scale the WPS of the continuum with that of the line *at the smallest scales* where the noise also dominates in the line. The normalized WPS so obtained for the continuum is then subtracted from the emission-line WPS. An example of such noise correction is shown in Figure 7.

The small-scale part of the WPS is very dependent on the noise in the data (see Fig. 8). The amount of noise is critical in our ability to identify *intrinsic* small-scale structures. Below some limiting scale, subtraction of noise effects becomes increasingly unreliable in determining the exact, intrinsic WPS, because intrinsic structures become indistinguishable from the noise. This *noise limit* is defined as the scale for which the noise component and the intrinsic component of the data reach the same amplitude in the WPS (see Fig. 7). The noise limit clearly identifies the scale below which any interpretation about the presence or behavior of intrinsic structures becomes hazardous.

If we are specifically looking for scaling laws, we must sample the largest possible significant range in scale, in order to derive anything useful. This significant range is set between the dominant scale and the noise limit. Therefore, increasing the accuracy in the detection and determination of scaling laws requires one to improve *both* the spectral resolution *and* the signal-to-noise ratio of the data, in order to have the noise limit set to smaller scales. Future observations should emphasize this goal, as well as providing better time resolution, in order to avoid any smearing out of

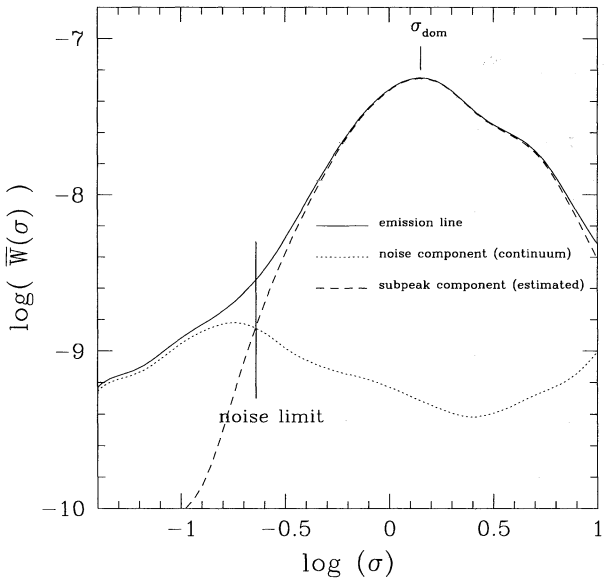

FIG. 7.—WPS for the subpeaks in the C III emission line of the WC7 star WR 137. The dominant scale σ_{dom} (see text) is defined as the scale σ where a maximum is reached. A WPS evaluated in the continuum region next to the line is used to determine the power contribution of the noise. This contribution is then subtracted from the subpeak power spectrum. The *noise limit* is defined as the lowest scale where the power contribution from the subpeaks can be evaluated with confidence.

the small-scale features because of their dynamical behavior.

5.3. *Fitting Data to the Model*

To test for the hypothesis of scaling behavior in emission-line subpeaks, we compare WPS obtained from the data to those of simulated profiles generated in accordance with the model described by equations (5)–(7), and to which a large-scale cutoff was included, in order to reproduce the presence of a dominant scale.

Three aspects of the observed and model wavelet spectra are compared: (1) the dominant scale σ_{dom}, (2) the power at the dominant scale $\bar{W}(\sigma_{dom})$, and (3) the scaling parameter $2\alpha + \beta$. The parameters σ_{dom} and $\bar{W}(\sigma_{dom})$ affect the WPS in the simplest way. In log-log space, they correspond to horizontal and vertical shifts. Only the scaling parameter $2\alpha + \beta$ directly reflects the *shape* of the WPS.

We have already shown the distinct scaling behavior we get by using triangles instead of Gaussians. Since other tested shapes led to a behavior intermediate between Gaussian and triangles, we restricted ourselves to two series of models, one using Gaussians, the other triangles. For each preassigned value of the parameter $2\alpha + \beta$ and for each fundamental shape (Gaussian or triangular), a set of synthetic signals was constructed. Individual values of α and β do not matter here, since only the combined parameter $2\alpha + \beta$ dictates the behavior of the associated WPS. For each set, the power spectrum was evaluated and compared to that previously found for the data. Synthetic power spectra were translated in log-log space based on least-squares fit procedures. For each star, we determined the model that fitted best the observed WPS (e.g., Fig. 9). Table 2 shows the parameters for the best-fitted model for each star. Gaussian and triangular models were treated separately, and results are given for each type. Because moderately high values of $\phi(2\alpha + \beta)$ are found, the two models do not lead to the same value of $2\alpha + \beta$ (see Fig. 4).

We note here that decoupled values of α and β cannot be determined using the current WPS technique. So far, we know of no way to determine their individual values other than by extracting and analyzing individual features in the data, a procedure we believe to suffer from various biases. We will, therefore, restrict ourselves to the determination of $2\alpha + \beta$, from which useful information can still be inferred.

5.4. *Discussion*

5.4.1. *Dominant Scales*

Table 2 shows the dominant scale σ_{dom} and its corresponding velocity dispersion σ_v found for the substructures

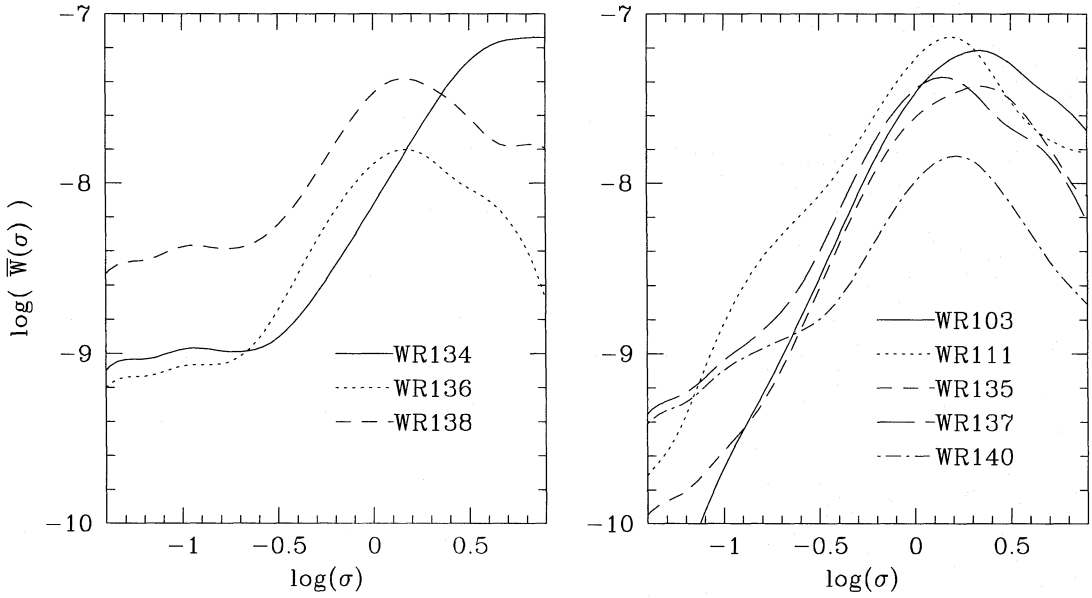

FIG. 8.—WPS from subpeaks of all W-R stars in the sample. The left panel refers to subpeaks observed in the He II λ5412 line; the right panel is for those observed in C III λ5696. The amplitudes were normalized in overall emission-line amplitude units, so that a comparison can be made between different stars. Notice the distinct shape of the WPS from star WR 134, and the various levels introduced by the noise in the low scale region.

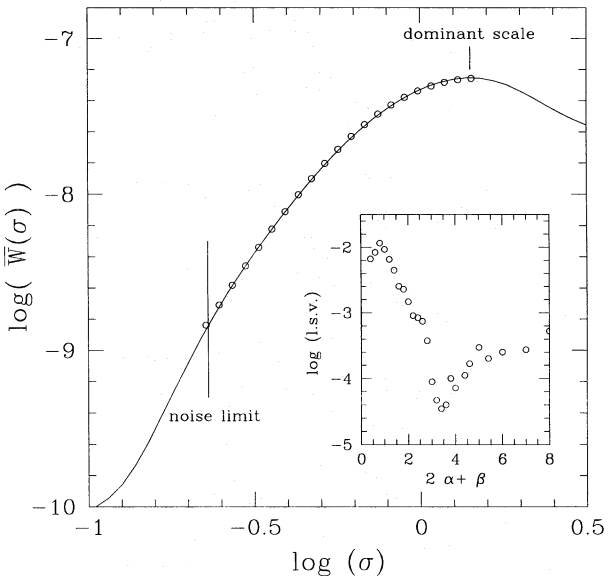

FIG. 9.—WPS of a subpeak model (*circles*) that best fits the WPS of subpeaks on the C III line in WR 137 (corrected for noise, *solid line*) between the noise limit and the dominant scale. The model uses a set of Gaussians (fundamental shape) with 1.7 Å (~90 km s^{-1}) as the dominant scale and a scaling parameter $2\alpha + \beta = 3.4$. The subplot shows the least-square value (lsv) obtained by fitting the WPS of similar models with given values of $2\alpha + \beta$; it clearly shows a minimum around $2\alpha + \beta = 3.4$.

in each star. The value of σ_v for the largest individual substructures present in the line tends to be relatively similar for most stars [94 ± 11(s.d.) km s^{-1}], except for WR 134.

The dominant scale for WR 134 is *much* larger, with $\sigma_v \sim$ 440 km s^{-1}. This suggests that at least some (i.e., the largest) of these subpeaks might have a different origin. Actually, it was already noticed by Robert (1992) and McCandliss et al. (1994) that the *largest* subpeaks in the lines of WR 134 move in a periodic fashion, in contrast to the apparently stochastic nature of all the subpeaks seen in other stars of the sample. This periodic behavior might be the result of asymmetry in a single rotating star or a binary system. This distinct-origin hypothesis is corroborated by the wavelet analysis.

The outstanding nature of WR 134 serves as supplemental evidence that there is no a priori reason for observing the same dominant scale in each of the other stars. The observed dominant scale seems to be an intrinsic property of WR stars as a whole, rather than some purely numerical phenomenon. Moreover, there is some evidence that a general stochastic phenomenon similar to that of the other stars is *also* present in WR 134 but superposed on the variations generated by the large-scale periodic behavior. The scaling parameter $2\alpha + \beta$ for WR 134 is small, indicating a significant subpeak component on smaller scales. We suggest that this arises in an additional subpeak distribution similar to that seen in other stars, that is superposed on the large periodic structures.

5.4.2. *Scaling Properties*

The interpretation of our results in terms of scaling laws is complicated by the fact that we are dealing with structures seen in projected velocity space. The widths of the subpeaks observed in the emission lines cannot be directly associated with the physical sizes of the corresponding wind inhomogeneities. Any density enhancement should have a minimal velocity dispersion because of its internal temperature. For a gas of (helium) ions in a hot (10^4 K) wind, this would be of the order of ~5 km s^{-1} (~0.1 Å in our lines), and no subpeak having smaller width should be observed. This makes our simple model, where σ can take any arbitrarily small value, unsuited to the observed phenomenon. However, since the resolution in our data is also 0.1 Å, our model can be used as a good approximation in the corresponding spectral regime, but a more complete physical model is still needed in order to relate the velocity dispersion σ_v to the real, physical extension of the subpeaks.

The most we can do with the current oversimplified model is to speculate about the total flux emitted by the intrinsic variable component in the line. According to our model, with a scaled distribution described by equations (6) and (7), the total flux emitted by any given scale $F(\sigma)d\sigma$ is proportional to $\sigma^{\alpha+\beta+1}\,d\sigma$ (eq. [8]). Hence, if the coefficient $\alpha + \beta + 1$ is greater than 0, then most of the flux will arise in the largest structures, but if it is smaller than 0, then most of the flux will be emitted by the small structures. In the latter case, the large subpeaks observed are seen as the "tip of the iceberg," and a much larger part of the flux in the emission line might come from (smaller) density enhancements; this has already been suggested by Moffat & Robert (1994). In the former case, however, the small density enhancements (if any) are not bright enough or numerous enough to make a significant contribution as a whole. In this case, most of the observed line flux would arise in another (likely *smooth*) component of the wind.

These possibilities are illustrated in Figure 10, where the previous (biased, i.e., not allowing for superposition effects) values obtained for the parameters α and β and the current range of estimates are plotted. Note that the range of old values does not agree with the current estimates, which means that, assuming the present analysis to be viable, the various biases we suspected to be present effectively led to an erroneous evaluation of the scaling parameters. Figure 10 also shows the zones for which these parameters would

TABLE 2

BEST-FIT SUBPEAK MODEL PARAMETERS

Star	σ_{dom} (Å)	σ_v (km s^{-1})	$\bar{W}(\sigma_{dom})$	$2\alpha + \beta$ (Gaussians)	$2\alpha + \beta$ (Triangles)
WR 103.....	2.0 ± 0.1	105 ± 5	0.029	2.5 ± 0.2	3.3 ± 0.5
WR 111.....	2.0 ± 0.1	105 ± 5	0.033	2.3 ± 0.2	2.9 ± 0.3
WR 134.....	8.0 ± 1.5	440 ± 80	0.032	1.2 ± 0.1	1.7 ± 0.3
WR 135.....	1.8 ± 0.1	95 ± 5	0.021	2.6 ± 0.2	3.5 ± 0.5
WR 136.....	1.5 ± 0.2	83 ± 11	0.015	2.8 ± 0.2	3.2 ± 0.5
WR 137.....	1.5 ± 0.2	79 ± 11	0.025	3.4 ± 0.4	4.5 ± 1.0
WR 138.....	1.6 ± 0.2	88 ± 11	0.025	2.5 ± 0.6	3.0 ± 0.5
WR 140.....	1.9 ± 0.2	100 ± 11	0.014	>4	>5

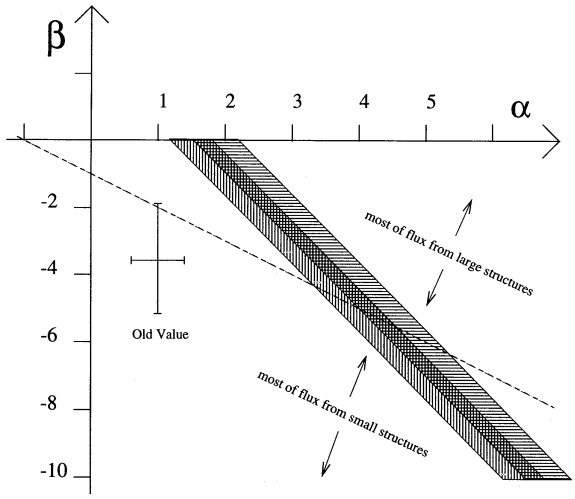

FIG. 10.—Plot showing the range of model parameters α and β that are consistent with the data. Vertical shading shows the results obtained when using the model with Gaussian subpeaks, horizontal shading for the model with triangular subpeaks. The dashed line separates parameter space in regions where the flux contribution is dominated by small- and large-scale structures, as indicated. The error bars shows the range of values obtained with previous techniques (extracted subpeaks), which are believed to suffer from various biases.

indicate a large-scale or small-scale flux-dominated distribution. We observe that values of $\alpha \lesssim 4$ and $\beta \gtrsim -5$ that lie within the allowed shaded regions would lead to a large-scale flux-dominated regime, where the (undetectable) small-scale part of the distribution does not contribute enough flux to account for a significant fraction of the line flux. The converse is possible, though, if $\alpha \gtrsim 4$ and $\beta \lesssim -5$ within the allowed region. However, the latter case makes the model appear to be somewhat *ad hoc*, and a different model might be more appropriate. In any case, this raises doubts about the hypothesis of a fully clumped wind that assumes that most (or all) of the line flux arises in an inhomogeneous component (Moffat & Robert 1994). We speculate that more sophisticated subpeak models, perhaps involving no scaling laws, could also be consistent with the data. The wavelet technique presented here could be used as an objective test for these alternative models.

Further investigations should be carried out by gathering spectra with finer spectral resolution in order to test for scaling properties of the line structure to smaller scales. The intrinsic velocity dispersion arising in thermal broadening might, however, set an inescapable low-scale limit to such a detection. New observations should be made with a simultaneous increase in spectral and time resolution as well as S/N. From the current wavelet power spectra, we estimate that gaining, say, an additional threefold in scale can only be achieved by increasing the spectral resolution by a factor of 3, and the signal-to-noise ratio by a factor of 10. In order to increase the time resolution by a factor of 3 as well (see paper II), this would require observing bright stars ($m < 3$) with a large telescope ($\phi > 3$ m).

6. SUMMARY AND PERSPECTIVES

We have presented a new objective technique to analyze the stochastic variable emission component in line spectra of Wolf-Rayet stars, involving the use of a *wavelet power spectrum* (WPS). This technique was used to quantify the intrinsic variable component in the line and to test for consistency with the idea of scaling laws.

The data were found to be increasingly affected on smaller scales by instrumental and statistical noise. The WPS was used to determine a *noise limit*, defining the scale below which the data became unreliable because of the noise. The effects of the noise on the WPS were evaluated and statistically removed.

We have identified a scale where the WPS reaches a maximum, the *dominant scale*, which is presented as a new parameter to characterize the variable subpeak component in the emission line. The dominant scale is found to be similar in most of the stars of our sample, suggesting that the variable subpeaks in these stars have a similar origin. The only exception is in the star WR 134, where a larger dominant scale corroborates previous results indicating a distinct nature for the observed subpeaks (Robert 1992; McCandliss et al. 1994). Further studies should include a larger sample of Wolf-Rayet stars, where the dominant scale should be checked in lines of various ionization levels. This is required to search for any correlation between the dominant scale and the most obvious stellar parameters, such as the wind terminal velocity, the spectral subclass, or the mass-loss rate.

We have introduced a simple phenomenological model for the variable subpeak component, describing it as a sum of Gaussian-like features of various scales σ (eq. [5]). The model allows for the presence of scaling laws, in the form of power laws parameterized by the powers α and β (eqs. [6] and [7]). We have shown that only the combined parameter $2\alpha + \beta$ can be safely estimated from the WPS. We have found the data to be consistent with our model, providing $2\alpha + \beta \approx 2.7 \pm 0.4$(s.d.) for Gaussian subpeaks, and $2\alpha + \beta \approx 3.4 \pm 0.6$(s.d.) for triangular subpeaks, neglecting WR 134 and WR 140 in both cases. Other subpeak shapes are believed to give intermediate results. We have noted the possibility that other models might give slightly different scaling properties, including the possibility that no scaling laws are present. The WPS technique is expected to be a good way to test for other (more physical) subpeak models.

So far, the information contained in the time evolution of the subpeaks, as well as systematic variations in the behavior of the subpeaks across a single emission line, has not been considered. This will be considered in Paper II.

In order to increase our confidence in the above results, an increase in the range of scales over which subpeaks can be identified (roughly between the dominant scale and the noise limit) is required. So far, because of noise limitations, we are not able to observe scaling behavior over more than 1 order of magnitude in scale. Improved, but difficult observations are necessary, using increased spectral and time resolution combined simultaneously with better signal-to-noise ratio, in order to push the noise limit several factors lower. High time resolution may also be required for a better identification of individual subpeaks, in order to determine their fundamental shape. We would then expect to obtain more significant results for the scaling properties of emission-line subpeaks in Wolf-Rayet stars. This would place us in a better position to evaluate the true impact of clumping on basic key quantities such as the mass-loss rate.

The authors are grateful to J. C. Brown, A. Conway, and L. Richardson from Glasgow University, for useful, constructive comments and discussions related to this work.

S. L. acknowledges the support provided by a Post-Graduate Scholarship from NSERC of Canada. A. F. J. M. and R. N. H. are grateful to NSERC of Canada (A. F. J. M. is also grateful to FCAR Québec) for financial aid.

REFERENCES

Annuk, K. 1991, in IAU Symp. No. 143, Wolf-Rayet Stars and Interrelations with Other Massive Stars in Galaxies, ed. K. A. van der Hucht & B. Hidayat (Dordrecht: Reidel), 245
Antokhin, I. I., Kholtygin, A. F., & Cherepashchuk, A. M. 1988, AZh, 65, 558
Antokhin, I. I., Nugis, T., & Cherepashchuk, A. M. 1992, AZh, 69, 516
Argoul, F., Arnéodo, A., Elezgaray, J., Grasseau, G., & Murenzi, R. 1989, Phys. Lett. A, 135, 327
Brown, J. C., Richardson, L. L., Antokhin, I. I., Robert, C., Moffat, A. F. J., & St.-Louis, N. 1995, A&A, 295, 725
Cherepashchuk, A. M., Eaton, J. A., & Khaliullin, K. F. 1984, ApJ, 281, 774
Daubechies, I. 1992, Ten Lectures on Wavelets (Philadelphia: SIAM)
Farge, M. 1992, Ann. Rev. Fluid Mech., 24, 395
Gill, A. G., & Henriksen, R. N. 1990, ApJ, 365, L27
Henriksen, R. N. 1991, ApJ, 377, 500
Hillier, D. J. 1991, A&A, 247, 455
Lépine, S. 1994, Ap&SS, 221, 371
Lépine, S., et al. 1996, in preparation (Paper II)
Martínez, V. J., Paredes, S., & Saar, E. 1993, MNRAS, 260, 365
McCandliss, S. R. 1988, Ph.D. thesis, Univ. Colorado, Boulder
McCandliss, S. R., Bohannan, B., Robert, C., & Moffat, A. F. J. 1994, Ap&SS, 221, 155
Moffat, A. F. J., Drissen, L., Lamontagne, R., & Robert, C. 1988, ApJ, 334, 1038
Moffat, A. F. J., Lépine, S., Henriksen, R. N., & Robert, C. 1994, Ap&SS, 216, 55
Moffat, A. F. J., & Robert, C. 1994, ApJ, 421, 310
Prinja, R. K., Barlow, M. J., & Howarth, I. D. 1990, ApJ, 361, 607
Robert, C. 1992, Ph.D. thesis, Univ. Montréal
Slezak, E., De Lapparent, V., & Bijaoui, A. 1993, ApJ, 409, 517
Slezak, E., Durret, F., & Gerbal, D. 1994, AJ, 108, 1996
Szatmáry, K., Vinkó, J., & Gál, G. 1994, A&AS, 108, 377
Van der Hucht, K. A., Conti, P. S., Lundstrom, & I., Stenholm, B. 1981, Space Sci. Rev., 28, 227